Anomalous Transport Properties in BiS2-based Superconductors LnO1−xFxBiS2 (Ln = Nd, La-Sm)

Anomalous Transport Properties in BiS_2-based Superconductors $LnO_{1-x}F_xBiS_2$ (*Ln* = Nd, La-Sm)

Sho Iwasaki[1], Yoshiki Kawai[1], Shotaro Takahashi[1], Takaya Suda[1], Ying Wang[1], Yasunori Koshino[1], Fumiya Ogura[1], Yoshiyuki Shibayama[1], Tohru Kurosawa[2], Migaku Oda[2], Masayuki Ido[2], and Naoki Momono[1] *

[1]*Applied Physics Course, Muroran Institute of Technology, Muroran, Hokkaido 050-8585, Japan*

[2]*Department of Physics, Hokkaido University, Sapporo, Hokkaido 060-0810, Japan*

We report the electronic properties of the layered bismuth-based sulfide superconductors $NdO_{1-x}F_xBiS_2$ (x = 0.25, 0.4, and 0.5) and $La_{1-y}Sm_yO_{0.5}F_{0.5}BiS_2$($y$ = 0.1 – 0.7), which have been studied by investigation of their transport properties and X-ray diffraction. In the lightly carrier-doped $NdO_{1-x}F_xBiS_2$(x = 0.25 and 0.4) and $La_{1-y}Sm_yO_{0.5}F_{0.5}BiS_2$($y$ = 0.3 and 0.4), the resistivity and Hall coefficient exhibit anomalous temperature dependences below $T_{CDW} \sim 130$ and 200 K, respectively, suggesting the formation of an energy gap on the Fermi surface associated with charge-density wave (CDW). In $NdO_{1-x}F_xBiS_2$(x = 0.25), the bond angles and bond length of the Bi-S pentahedron change their temperature dependences below $\sim$ 200 K, suggesting that a lattice instability related to the Bi-S pentahedron exists below $\sim$ 200 K, which is much higher than T_{CDW}. These results indicate that the lattice instability of the Bi-S pentahedron can trigger a CDW transition in the low-carrier region of BiS_2 superconductors.

*mom@mmm.muroran-it.ac.jp

1. Introduction

The typical BiS_2-based layered superconductor $LnO_{1-x}F_xBiS_2$ (*Ln*: La, Ce, Pr, Nd, Sm, and Yb) has attracted considerable attention since $Bi_4O_4S_3$ and *Ln* = La ($LaO_{1-x}F_xBiS_2$) were discovered in 2012.[1–7] These compounds have similar crystal structures to high-temperature superconductors such as iron pnictide superconductors.[8] The crystal structure is composed of alternately stacked superconducting layers (double BiS_2 layers) and blocking layers ($LnO_{1-x}F_x$).[1] The parent compounds of most BiS_2-based superconductors are semiconductors.[9] The superconductivity emerges owing to carrier doping into the BiS_2 layers by substituting F^- for O^{2-} in $LnO_{1-x}F_x$ layers. The carrier doping can also be induced by valence fluctuation at the *Ln* site, as reported for $CeOBiS_2$, leading to the emergence of superconductivity without the fluorine substitution.[10] The superconducting transition temperature T_c of $LnO_{1-x}F_xBiS_2$ depends on the fluorine concentration x and pressure.[9] The maximum T_c is about 10 K for high-pressure-annealed samples of $LaO_{0.5}F_{0.5}BiS_2$.[11] It was found by theoretical calculation that the topology of the Fermi surface (FS) changes from an electron-like FS around the Brillouin zone boundary to a hole-like one around the Γ point at $x = 0.5$. The hole-like FS has good nesting conditions.[12,13] The relationship between the charge-density wave (CDW) instability and the superconductivity in this system is of much interest. The temperature dependence of resistivity $\rho(T)$ for $LnO_{1-x}F_xBiS_2$ depends on the carrier concentration and pressure. In $LaO_{1-x}F_xBiS_2$, $\rho(T)$ for $x \sim 0.23$ exhibits semiconducting behavior above T_c, whereas $\rho(T)$ for $x \sim 0.46$ exhibits metallic behavior.[14] Furthermore, the semiconducting behavior of $\rho(T)$ at ambient pressure is suppressed by applying high pressure to $LaO_{1-x}F_xBiS_2$ and $La_{1-y}Sm_yO_{0.5}F_{0.5}BiS_2$.[11,15] For $NdO_{1-x}F_xBiS_2$, it was reported that $\rho(T)$ for $x = 0.3$ exhibits metallic behavior, as well as that for $x \sim 0.5$,[16–20] indicating that $\rho(T)$ is more metallic in $NdO_{1-x}F_xBiS_2$ than in $LaO_{1-x}F_xBiS_2$. This tendency has been considered to be related to the variation of the packing density in the BiS_2 layers, which is caused by the difference in the ionic radius between La and Nd atoms (the so-called in-plane chemical pressure).[21,22] Semiconducting behavior of $\rho(T)$ was also reported in lightly carrier-doped $La_{1-x}M_xOBiS_2$(M=Ti, Zr, Hf, and Th).[23] Yazici *et al*. reported that $\rho(T)$ shows inflectional behavior in its semiconducting temperature dependence around ~120 K, and pointed out that the inflection could be related to a CDW instability.[23] However, the origin of the inflection in $\rho(T)$ has not yet been clarified.

The difference in the electronic states between *Ln* = La and Nd has also been investigated from the viewpoint of the FS topology. In $LaO_{1-x}F_xBiS_2$, the change from the electron-like

FS to the hole-like FS with increasing x has been revealed by angle-resolved photoemission spectroscopy (ARPES).[24,25] On the other hand, the electron-like FS around the Brillouin zone boundary has been observed in samples of $NdO_{1-x}F_xBiS_2$ with $x = 0.16$,[19] 0.29,[26] and 0.44.[27] Moreover, it was reported that the carrier concentration is clearly lower than that expected from the fluorine concentration at $x = 0.5$.[19] The theoretical calculation suggested a good FS nesting condition for the hole-like FS.[12,13] However, a modulation structure has been revealed in $NdO_{1-x}F_xBiS_2$ with low carrier concentration by scanning tunneling microscopy, although it is unclear whether the modulation observed on the cleaved surface of $NdO_{1-x}F_xBiS_2$ has a bulk nature.[28] In addition, in-plane local distortions owing to the in-plane displacement of sulfur atoms were found in $NdO_{1-x}F_xBiS_2$ by neutron diffraction and pair density function analyses.[29] It is considered that the in-plane sulfur displacement may be related to CDW instability.[30] It is important to discuss the local distortion and electronic states in $NdO_{1-x}F_xBiS_2$. As mentioned above, the large hole-like FS in $LaO_{1-x}F_xBiS_2$ with $x = 0.46$ was confirmed experimentally by ARPES, which is in sharp contrast to that in $NdO_{1-x}F_xBiS_2$. However, it is still unclear if CDW instability exists in $LaO_{1-x}F_xBiS_2$ with $x \sim 0.5$, although lattice distortions around Bi atoms in the BiS_2 plane were reported to exist.[31]

In $LnO_{1-x}F_xBiS_2$, the effects of a large chemical pressure on T_c have been studied so far.[9,21,32] It was reported that the chemical pressure within the BiS_2 plane plays an important role in determining T_c.[21] It is important to investigate how the chemical pressure affects the electronic properties in the normal state, which have CDW instability, in order to understand the mechanism of superconductivity in BiS_2-based superconductors.

In this paper, we report the electronic properties of $NdO_{1-x}F_xBiS_2$ and $La_{1-y}Sm_yO_{0.5}F_{0.5}BiS_2$. In $NdO_{1-x}F_xBiS_2$ ($x = 0.25$, 0.4, 0.5) and $La_{1-y}Sm_yO_{0.5}F_{0.5}BiS_2$ ($y = 0.1 \sim 0.7$), transport properties such as ρ and R_H exhibit small anomalies below $\sim$ 130 and $\sim$ 200 K, respectively. These small anomalies can be ascribed to the formation of an energy gap on part of an FS. Furthermore, in $NdO_{1-x}F_xBiS_2$ ($x = 0.25$), the bond angles and bond lengths of the Bi-S pentahedron change their temperature dependences below $\sim$ 200 K, where $R_H(T)$ for $x = 0.25$ starts to increase gradually with decreasing temperature. This suggests that in lightly carrier-doped samples, some kind of lattice instability related to the Bi-S pentahedron can exist below $\sim$ 200 K, which triggers a CDW transition with the energy gap opening on part of an FS.

2. Experiments

Single crystals of $NdO_{1-x}F_xBiS_2$ and $La_{1-y}Sm_yO_{0.5}F_{0.5}BiS_2$ were grown in a quartz tube sealed in vacuum by the CsCl/KCl flux method.[16] For $NdO_{1-x}F_xBiS_2$, the raw materials were Nd_2S_3, Bi_2S_3, Bi_2O_3, BiF_3, and Bi, which were weighted with nominal compositions of $x = 0.25$, 0.4, and 0.5. The ratio of the sample to the flux was 1:3.75 (sample:flux) at $x = 0.25$ and 0.4 and 1:7.5 at $x = 0.5$. For $La_{1-y}Sm_yO_{0.5}F_{0.5}BiS_2$, the raw materials were La_2S_3, BiF_3, SmF_3, Sm_2O_3, Sm_2S_3, Bi_2O_3, Bi_2S_3, and Bi for $y = 0.1 - 0.7$. These starting materials were weighted with nominal compositions of $y = 0.1 - 0.7$. The ratio of the sample to the flux was 1:7.5. The heating temperature and cooling rate were modified for each sample. For $NdO_{1-x}F_xBiS_2$, the samples with $x = 0.25$, 0.4, and 0.5 were heated for 10 – 12 h at 800 – 950 °C, then cooled to 600 °C at a rate of 0.5 – 1.0 °C/h. For $La_{1-y}Sm_yO_{0.5}F_{0.5}BiS_2$, the samples were heated for 12 h at 900 °C, then cooled to 600 °C at a rate of 0.5 – 1.0 °C/h for $x = 0.1 - 0.7$. We performed single-crystal X-ray diffraction experiments from $\sim$ 290 to $\sim$ 120 K using a Rigaku Varimax Saturn CCD diffractometer (Rigaku, Inc.). The temperature dependence of magnetization was measured using a superconducting quantum interference device magnetometer (Quantum Design, Inc.) with an applied field of 3 Oe along the c-axis. The temperature dependences of the resistivity $\rho(T)$ along the ab-plane and the Hall coefficient $R_H(T)$ were measured by the four-terminal method using a Physical Property Measurement System (Quantum Design, Inc.). The $R_H(T)$ measurements were performed by turning samples over with a magnetic field of 5 T applied along the c-axis. The temperature dependence of the Seebeck coefficient $S(T)$ along the ab-plane was measured by an ordinary two-probe method using a laboratory-made measurement system. Two 0.07% AuFe-chromel thermocouples of 0.20 mm diameter (Iwatani Co.) were attached to the sample using Ag paste (Du Pont, 4922N). The Seebeck coefficient of the chromel wire was calibrated in advance using a 99.999% lead wire.[33] A 120 Ω strain gauge was employed as a heater to provide a temperature gradient in the sample. The maximum temperature gradient was not more than 5% of the sample temperature.

Table I shows the results of composition analyses using an electron probe microanalyzer (EPMA) and by X-ray diffraction experiments. The chemical ratio of Nd to Bi estimated using the EPMA nearly agrees with the stoichiometry for $x = 0.25$, 0.4, and 0.5. The chemical ratios estimated using the EPMA are comparable to the site occupancies in the structure analyses as shown later.

3. Results and Discussion

3.1 $NdO_{1-x}F_xBiS_2$

The structure analyses by X-ray diffraction experiments at room temperature (~ 290 K) show that the crystal structure possesses tetragonal symmetry with the space group $P4/nmm$ at $x = 0.25$, 0.4, and 0.5. The refinement of the structure is performed as $NdOBiS_2$, because oxygen and fluorine are light elements. The occupancies at Bi, S1 (in-plane), and S2 (out-of-plane) sites, normalized by Nd site occupancy, are shown in Table I; the occupancies at these sites are ~1.0. The results shown in Table I suggest that the $NdO_{1-x}F_xBiS_2$ crystals in this study are almost stoichiometric for Nd, Bi, S1, and S2.

Figure 1 shows the x-dependences of a-axis and c-axis lengths in this study, together with those reported in other studies.[4,16,17,27] The a-axis length is nearly independent of x and averages to 3.993 Å. The c-axis length decreases monotonically with increasing x. As shown in Fig. 1, the x-dependence of the c-axis length is slightly different between the data for nominal and net x above $x > 0.4$. From Fig. 1, the deviation of net x from nominal x can be roughly estimated to be ~0.1 for the present $NdO_{1-x}F_xBiS_2$ crystals with x=0.4 and 0.5. Demura *et al*. reported that $NdO_{1-x}F_xBiS_2$ has a solubility limit between $x = 0.4$ and 0.5.[4] The deviation of net x for the present $NdO_{1-x}F_xBiS_2$ crystals with x=0.4 and 0.5 may be related to the solubility limit.

Figure 2(a) shows the temperature dependence of magnetic susceptibility. The superconducting transition temperature (T_c^M) was defined as the onset of a diamagnetic signal. T_c^M is approximately 5 K at nominal $x = 0.25$, 0.4, and 0.5. Figure 2(b) shows the temperature dependence of $\rho(T)$ from 2 to 10 K. Zero resistance was observed at $T_c^{zero} = 4.6$ K for $x = 0.25$ and 0.5 and at 4.8 K for $x = 0.4$. There is no significant difference in T_c for $x = 0.25$, 0.4, and 0.5.

Figure 3(a) shows the temperature dependence of $\rho(T)$ along the ab-plane from 2 to 300 K. ρ(300 K) is 1.3 mΩcm for $x = 0.25$ and 0.54 mΩcm for $x = 0.5$; roughly speaking, the lower the resistance, the higher the nominal x-value. This result implies that the carrier concentration increases with increasing x. $\rho(T)$ for $x = 0.5$ exhibits metallic behavior over the entire T-range above T_c. $\rho(T)$ for $x = 0.25$ and 0.4 also exhibits metallic T-dependences at high temperatures. Note that $\rho(T)$ for $x = 0.25$ and 0.4 exhibits slight upturns below ~ 130 K and tends to be metallic again below ~ 40 K. In other words, $\rho(T)$ for $x = 0.25$ and 0.4 increases slightly between ~ 40 and ~ 130 K. It seems difficult to explain the behaviors of $\rho(T)$ for $x = 0.25$ and 0.4 from the viewpoint of a carrier localization scenario owing to some kind

of disorder. The increase in resistivity between ~ 40 and ~ 130 K in $NdO_{1-x}F_xBiS_2$ (x = 0.25, 0.4) is qualitatively similar to that of $EuBiS_2F$ reported by Zhai *et al.*,[34] although the temperature (~ 280 K) at which $\rho(T)$ of $EuBiS_2F$ shows the increase is much higher than those of $NdO_{1-x}F_xBiS_2$ with x = 0.25 and 0.4 in this study. Zhai *et al.* reported that the anomalous temperature dependence of $\rho(T)$ in $EuBiS_2F$ can be ascribed to a dynamic/short-range CDW ordering. For $EuBiS_2F$, it was reported that the Hall coefficient also shows anomalous T-dependence. Then we also measured the Hall coefficients of $NdO_{1-x}F_xBiS_2$ crystals with x = 0.25, 0.4, and 0.5 to investigate the nature of the electronic states in $NdO_{1-x}F_xBiS_2$ in more detail.

Figure 3(b) shows the temperature dependence of the Hall coefficient, $R_H(T)$, along the *ab*-plane, measured under a magnetic field of 5 T along the *c*-axis. The R_H(290 K) values for x = 0.25, 0.4, and 0.5 are negative: -1.9×10^{-3}, -1.7×10^{-3}, and -0.76×10^{-3} cm^3/C, respectively. The absolute value of R_H(290 K) is smaller for x = 0.5 than for x = 0.25. This result qualitatively supports the fact that the carrier concentration of the present $NdO_{1-x}F_xBiS_2$ crystals increases with the increase in nominal x. If we simply assume a single-band scenario, the carrier density at 290 K is estimated to be $n = 1/|eR_H|$ = 0.33, 0.37, and 0.82×10^{22} cm^{-3} for x = 0.25, 0.4, and 0.5, leading to n = 0.35, 0.39, and 0.88 electrons/formula unit for x = 0.25, 0.4, and 0.5, respectively. The n-values for x = 0.25 and 0.4 are not so far from their x, even though net x (~0.3) is used for x=0.4. On the other hand, the n-value for x = 0.5 is considerably different from x, meaning that the electronic states for x = 0.5 are far from a single-band picture.

$R_H(T)$ for x = 0.5 increases with decreasing temperature and crosses zero at ~ 200 K. The zero-crossing temperature in $R_H(T)$ slightly decreases with increasing x. One of the possible origins for the temperature-dependent $R_H(T)$ is multi-carriers with different natures. However, the origin and mechanism of the temperature-dependent $R_H(T)$ in BiS_2-based superconductors have not yet been clarified. In the present crystals with x = 0.5, $\rho(T)$ exhibits metallic behavior over the entire T-range and no obvious anomaly. In addition, at high temperatures (> 200 K), where $\rho(T)$ for x = 0.25 and 0.4 show metallic behavior, $R_H(T)$ for x = 0.25 and 0.4 shows a similar temperature dependence to that of x = 0.5. Then, we assume that the temperature dependence of $R_H(T)$ for x = 0.5 is the normal one for $NdO_{1-x}F_xBiS_2$ when the electronic system shows no anomalous behavior. Interestingly, $R_H(T)$ increases more steeply for x = 0.25 and 0.4 than for x = 0.5 at low temperatures. The large increases in $R_H(T)$ for x = 0.25 and 0.4 are similar to the anomalous temperature dependence of $R_H(T)$ in $EuBiS_2F$, which was reported to originate from FS reconstruction due to CDW transition.[34]

To estimate the temperature where the anomalous behavior of the electronic properties occurs, we compare the ρ and R_H data of $x = 0.25$, 0.4, and 0.5 in more detail. Figure 4(a) shows the normalized resistivity $\rho(T)/\rho(150\ \mathrm{K})$ for $x = 0.25$, 0.4, and 0.5. The normalized $\rho(T)$ values are in good agreement with each other over a wide T-range above ∼130 K, whereas the normalized data for $x = 0.25$ and 0.4 deviate from that of $x = 0.5$ below ∼130 K. Figure 4(b) shows $\Delta R_H(T)$, which is defined as $\Delta R_H(T) = R_H(T, x) - R_H(T, x = 0.5)$. $\Delta R_H(T)$ is almost constant at high temperatures. $\Delta R_H(T)$ starts to increase gradually below ∼ 200 K and steeply below ∼ 130 K. The characteristic temperatures (T_{CDW}) where $\rho(T)$ and $R_H(T)$ show the upturns agree with each other; T_{CDW} ∼ 130 K, as shown in Fig. 4. In addition, $\rho(T)$ for $x = 0.25$ and 0.4 show metallic temperature dependences below ∼ 40 K, where $\Delta R_H(T)$ also tends to be saturated. These results indicate that the electronic properties exhibit anomalous behaviors between ∼ 40 and ∼ 130 K, which can be ascribed to the gap evolution on a part of the FS due to CDW formation.

The CDW formation is usually accompanied by the development of an energy gap on part of an FS. If we assume that the scattering rate of the carriers, namely, relaxation time, is not changed significantly below ∼ 130 K, we can estimate the area where the FS disappears on the basis of the energy gap opening from the normalized resistivity below ∼ 130 K in Fig. 4(a); the gapped areas of the FS are ∼11 and ∼8% for $x = 0.25$ and 0.4, respectively. These values are comparable to that of $EuBiS_2F$ (∼10%) if we can use a similar estimation method to that reported by Zhai *et al.*[34] These results suggest that the nested area of the FS is similar between $EuBiS_2F$ and $NdO_{1-x}F_xBiS_2$ ($x = 0.25$ and 0.4).

The CDW is accompanied by some kind of lattice distortion. To investigate the relationship between the anomalous transport properties and the nature of the lattice distortion, the structure refinements at $x = 0.25$ were performed from ∼ 120 K to room temperature (∼ 290 K) by single-crystal X-ray diffraction experiments. The results of the structure refinements are summarized in Table II. In the T-range examined in the present study, the result of the structure refinement indicates the tetragonal structure with the space group $P4/nmm$. Figures 5(a) and 5(b) show the temperature dependences of the a-axis and c-axis lengths for $x = 0.25$, respectively. These lattice constants decrease with decreasing temperature, leading to the volume of the unit cell also decreasing with decreasing temperature. Here, we defined the in-plane sulfur as S1 and the out-of-plane sulfur as S2 [Fig. 5(c)]. Figure 5(d) shows the temperature dependences of the Bi-S1 and Bi-S2 distances. The Bi-S1 distance decreases monotonically with decreasing temperature over the entire T-range. On the other hand, the Bi-S2 distance increases linearly with decreasing temperature at high temperatures. Then, it

is saturated and decreases below ∼ 200 K, indicating that the bond length between the S2 and Bi atoms in the Bi-S pentahedron changes the temperature dependence below ∼ 200 K. Figure 5(e) shows the temperature dependences of the out-of-plane angles of S1-Bi-S1 and S1-Bi-S2 bonds. Both bond angles are almost independent of temperature above ∼ 200 K. However, the out-of-plane S1-Bi-S1 angle decreases with decreasing temperature below ∼ 200 K, whereas the S1-Bi-S2 angle increases. These changes in bond angles and bond lengths around the Bi atom indicate that the relative position of the Bi atom in the Bi-S pentahedron slightly changes towards the apical S2 atom below ∼ 200 K. In the BiS_2 compounds with low carrier concentration, it was reported that a zigzag buckled basal plane is formed in the Bi-S pentahedron.[14,30,35] Upon electron doping, the basal plane changes into a flat plane. In lightly doped $NdO_{0.75}F_{0.25}BiS_2$, the zigzag buckled basal plane is T-dependent and its dependence becomes stronger below ∼ 200 K. Figure 5(f) shows the temperature dependence of the in-plane S1-Bi-S1 angle. The in-plane S1-Bi-S1 angle is also independent of temperature at high temperatures. Then, the in-plane S1-Bi-S1 angle slightly decreases with decreasing temperature below ∼ 200 K, suggesting an in-plane displacement of the S1 atom. For $NdO_{1-x}F_xBiS_2$, it has been reported that there are local distortions due to charge fluctuations in the BiS_2 layers.[29] The sample with $x = 0.2$ (non-superconducting) possesses local distortion due to the local in-plane displacement of sulfur atoms, the so-called ferrodistortive structure.[29] The behaviors of the in-plane S1-Bi-S1 angle seem to be related to the ferrodistortive structure. In other words, the S1 atoms slightly move toward the in-plane direction.

Despite the changes in the bond angles and bond lengths in the Bi-S pentahedron below ∼ 200 K, the average structure of the entire crystal maintains the tetragonal symmetry with the space group $P4/nmm$. This result suggests a possibility that the displacements of Bi and S1 in the Bi-S pentahedron are related to the local distortion revealed by neutron diffraction.[29] Interestingly, $\Delta R_H(T)$ starts to increase gradually with decreasing temperature below ∼ 200 K. If the local distortion couples with a CDW instability, it will lead to CDW formation with an energy gap on the FS. Thus, the CDW transition due to the periodic local distortion may occur at $x = 0.25$ and 0.4. The possibility of the CDW transition in $EuBiS_2F$[34] has been pointed out. In $EuBiS_2F$, the carrier doping has been induced by the Eu valence, and the electron doping level corresponded to $x \sim 0.2$.[34] In $NdO_{1-x}F_xBiS_2$, the samples with $x = 0.25$ and 0.4 exhibit the emergence of an energy gap and the local distortion leading to CDW formation. It is suspected that the electron-phonon coupling constant is larger at low carrier concentrations in the $LnO_{1-x}F_xBiS_2$ system.

The energy gap develops on the FS, leading to the reduction in the density of states at

E_F. Therefore, it can be expected that T_c is suppressed owing to CDW formation. However, the T_c values of $x = 0.25$ and 0.4 are comparable to that of $x = 0.5$. The possibility that the intrinsic T_c may be higher than T_c^{zero} and T_c^M for $x = 0.25$ and 0.4 should be considered.

3.2 $La_{1-y}Sm_yO_{0.5}F_{0.5}BiS_2$

Figure 6 shows the plot of nominal Sm concentration versus net Sm concentration in $La_{1-y}Sm_yO_{0.5}F_{0.5}BiS_2$, estimated using EPMA. The net Sm concentration increases monotonically with increasing nominal y and tends to be saturated above nominal y=0.6, although the Sm concentration for y=0.5 shows a relatively large difference. The structure analyses by X-ray diffraction experiments at room temperature (~290 K) show that the crystal structure is tetragonal with the space group $P4/nmm$ in $La_{1-y}Sm_yO_{0.5}F_{0.5}BiS_2$ with y=0.1~ 0.7. Figure 7 shows the Sm-doping dependences of the a-axis and c-axis lengths in $La_{1-y}Sm_yO_{0.5}F_{0.5}BiS_2$. The a-axis length decreases with increasing y and tends to be saturated around $y = 0.5$. The c-axis length increases with increasing y and then steeply decreases above $y = 0.5$. The Sm-doping dependence of the a-axis length at a low Sm concentration can be explained in terms of the smaller ionic radius of Sm than that of La, which is known as a chemical pressure effect.[21,32] Such an in-plane compression by Sm doping results in vertical expansion; that is, the c-axis length increases with increasing y below $y = 0.5$, although it is unclear why the c-axis length steeply decreases above $y = 0.5$. The decrease in the c-axis length is so large that it cannot be explained in terms of the difference between the nominal and net Sm concentrations above y=0.5.

Figure 8 shows the Sm-doping dependence of T_c in $La_{1-y}Sm_yO_{0.5}F_{0.5}BiS_2$. T_c is almost constant up to $y = 0.4$ and steeply increases with increasing y above $y = 0.5$. The Sm-doping dependence of T_c can be understood on the basis of the so-called in-plane chemical pressure effect, as shown in Fig. 9.[21] In Fig. 9, the T_c data of other BiS_2 materials reported by Mizuguchi *et al*. are also plotted (dashed line) as a function of the in-plane chemical pressure for comparison.[21] The increase in T_c above $y = 0.5$ is in good agreement with those reported for other BiS_2 materials. Note that the c-axis length markedly decreases in the y-range where T_c increases, suggesting that the decrease in the c-axis length may be related to the increase in T_c, in addition to the in-plane chemical pressure effect.

Figure 10 shows the temperature dependence of in-plane resistivity $\rho(T)$ for $La_{1-y}Sm_yO_{0.5}F_{0.5}BiS_2$. Here, the data for various Sm concentrations are normalized by ρ(300 K). $\rho(T)$ for $y = 0.1$ exhibits metallic behavior over the entire T-range above T_c. $\rho(T)$ for $y = 0.2$ exhibits a slight upturn below $\sim$ 200 K. The upturn of $\rho(T)$ below $\sim$ 200

K becomes larger with the increase in y and less evident for $y > 0.5$. The typical upturn behaviors of $\rho(T)$ are different from those of $NdO_{1-x}F_xBiS_2$($x = 0.25$ and 0.4); the temperature at which $\rho(T)$ of $La_{1-y}Sm_yO_{0.5}F_{0.5}BiS_2$ starts to increase is much higher than that of $NdO_{1-x}F_xBiS_2$. The metallic behavior of $\rho(T)$ below $\sim$ 40 K, observed in $NdO_{1-x}F_xBiS_2$, was not observed in $La_{1-y}Sm_yO_{0.5}F_{0.5}BiS_2$ except for $y = 0.6$. $\rho(T)$ for $y = 0.6$ shows similar behavior to those of $NdO_{1-x}F_xBiS_2$($x = 0.25$ and 0.4), but the anomaly is very small in comparison with those of $NdO_{1-x}F_xBiS_2$($x = 0.25$ and 0.4). The overall temperature dependence for $y = 0.6$ is considered to be metallic. Note that $\rho(T)$ for $y = 0.2 \sim 0.4$ shows weak inflectional behaviors around 100$\sim$150 K. The inflectional behaviors of $\rho(T)$ are similar to those in lightly carrier-doped $La_{1-x}M_xOBiS_2$(M=Ti, Zr, Hf, and Th) reported by Yazici *et al.*[23] They pointed out a possibility that the inflection point could be related to a CDW instability, although it is still unclear. Then, to further investigate the electronic states from transport properties, we measured the in-plane Hall coefficient $R_H(T)$ and Seebeck coefficient $S(T)$ of $La_{1-y}Sm_yO_{0.5}F_{0.5}BiS_2$ crystals.

Figure 11 shows the $R_H(T)$ in $La_{1-y}Sm_yO_{0.5}F_{0.5}BiS_2$. As shown in the inset of Fig. 11, R_H(300 K) shows a systematic change as a function of Sm concentration; R_H(300 K) is a positive value for $y = 0.1$ and decreases with increasing y, resulting in a negative value for $y = 0.7$. This result means that Sm doping causes the decrease in the number of electron carriers doped by F doping. The decrease in the carrier-doping level by Sm doping in $La_{1-y}Sm_yO_{0.5}F_{0.5}BiS_2$ is due to a deviation of the Sm valence from the trivalent state. The temperature dependence of $R_H(T)$ also depends on Sm doping. $R_H(T)$ for $y = 0.1$ increases linearly with decreasing temperature, whereas $R_H(T)$ for $y = 0.3$ and 0.4 shows anomalous upturns around $T = 200$ K, which are similar to that observed in $NdO_{1-x}F_xBiS_2$ with $x = 0.25$. Note that $R_H(T)$ becomes T-independent for the sample with $y = 0.7$, which shows the highest T_c in the present study on $La_{1-y}Sm_yO_{0.5}F_{0.5}BiS_2$. This is mainly due to the in-plane chemical pressure effects.

Here, we compare $R_H(T)$ and $\rho(T)$ in $La_{1-y}Sm_yO_{0.5}F_{0.5}BiS_2$ in more detail. Figure 12 shows $\Delta R_H(T)$ in $La_{1-y}Sm_yO_{0.5}F_{0.5}BiS_2$, which is defined by $\Delta R_H(T) = R_H(T, y) - R_H(T, y = 0.1)$, as discussed for $NdO_{1-x}F_xBiS_2$. $\Delta R_H(T)$ is nearly constant at high temperatures. $\Delta R_H(T)$ for $y = 0.3$ and 0.4 markedly increases below $\sim$ 190 and $\sim$ 160 K, respectively. These characteristic temperatures of $\Delta R_H(T)$ for $y = 0.3$ and 0.4, defined as T_{CDW}, are comparable to the temperatures where $\rho(T)$ starts to increase with decreasing temperature, as in $NdO_{1-x}F_xBiS_2$. T_{CDW} for $y = 0.3$ and 0.4 seems to be higher than the temperatures of their inflection points in $\rho(T)$. The inflection points in $\rho(T)$ may be related to the temperature where the gap evolution on the FS is saturated. The results of $\Delta R_H(T)$ suggest that the upturns in $\rho(T)$ and $R_H(T)$ can

be ascribed to the formation of a gap on the FS owing to a CDW formation, as discussed for $NdO_{1-x}F_xBiS_2$.

Figure 13 shows the temperature dependence of the Seebeck coefficient $S(T)$ for $La_{1-y}Sm_yO_{0.5}F_{0.5}BiS_2$ with $y = 0.3$. Roughly speaking, $S(T)$ is proportional to temperature over the entire T-range. Here, we focus on the detailed temperature dependence of $S(T)$; $S(T)$ shows a small kink around $\sim$ 220 K and changes its slope slightly. This temperature ($\sim$ 220 K) is close to $T_{\rm CDW}$ for $y = 0.3$, at which $\rho(T)$ and $R_{\rm H}(T)$ for $y = 0.3$ show upturns. In addition, $S(T)$ also changes its slope around $T = 60$ K and decreases toward zero with decreasing temperature. As is well known, $S(T)$ is generally given by

$$S(T) = a\frac{C_{el}}{e} - \frac{1}{e}\frac{d\zeta}{dT},$$

where e, C_{el}, and ζ are the electron charge (-1.602×10^{-19} C), the specific heat of one electron, and the chemical potential of electrons, respectively. The coefficient a is a factor related to the dimensionality of the electron system. For a quasi-two-dimensional electron system in a metal, both the first and second terms are proportional to temperature, although the second term should be zero in the case of an ideal two-dimensional electron gas. The proportional coefficient of $S(T)$ is related to the density of states at the Fermi level. Generally speaking, the Seebeck coefficient is hardly affected by the lattice imperfections and distortions. Thus, the small kink around $\sim$ 220 K observed here reflects the intrinsic change in the electronic states such as the formation of an energy gap on part of the FS.

It was previously found by ARPES that the electronic system in the BiS_2 superconductors has a quasi-two-dimensional FS.[19,24–27] Here, we roughly estimate the decrease in the density of states at the Fermi level E_F due to the gap opening in $La_{1-y}Sm_yO_{0.5}F_{0.5}BiS_2$. We use the formula of $S(T)$ for a two-dimensional electron gas; $S(T) \propto C_{el}/e$, where $C_{el} = \gamma T$. γ is the electronic specific heat coefficient and proportional to the density of states at E_F. $S(T)$ above $\sim$ 220 K is roughly proportional to temperature and its slope is -2.0×10^{-2} μV/K^2. $S(T)$ below $\sim$ 60 K is also proportional to temperature and its slope is -1.5×10^{-2} μV/K^2. The difference in their slopes is 0.5×10^{-2} μV/K^2, namely, 25% of that above $\sim$ 220 K. This value corresponds to the decrease in the density of states at E_F by the formation of a gap on the FS. Assuming the mean-field $T_{\rm c}$ in the weak coupling limit, $\Delta T_{\rm c}/T_{\rm c0} = e^{-1/0.75} \sim 26\%$, where $T_{\rm c0}$ is the superconducting transition temperature without the decrease in the density of states at E_F owing to CDW formation. As mentioned above, $T_{\rm c}$ of $La_{1-y}Sm_yO_{0.5}F_{0.5}BiS_2$ with $y = 0.3$ is about 2.8 K, leading to $T_{\rm c0} \sim 10$ K. On the other hand, in $NdO_{1-x}F_xBiS_2$ with $x = 0.25$ and 0.4, the gapped area of the FS is estimated to be about $8 \sim 11\%$. If we

use similar procedures, $\Delta T_c/T_{c0}$ for $NdO_{1-x}F_xBiS_2$ with $x = 0.25$ and 0.4 can be estimated to be $\sim$ 33%, where we simply assume that the decrease in the density of states at E_F is proportional to the gapped area of the FS. Then, T_{c0} for $NdO_{1-x}F_xBiS_2$ ($x = 0.25$ and 0.4) is $\sim$ 15 K. These T_{c0} values correspond to the highest T_c in $LnO_{1-x}F_xBiS_2$ superconductors without CDW formation. However, the estimation of T_{c0} here is oversimplified. Presumably, this T_{c0} corresponds to the lower limit of the highest possible T_c in the $LnO_{1-x}F_xBiS_2$ system.

4. Summary

The resistivity $\rho(T)$ and Hall coefficient $R_H(T)$ for $NdO_{1-x}F_xBiS_2$ ($x = 0.25$ and 0.4) and $La_{1-y}Sm_yO_{0.5}F_{0.5}BiS_2$ ($y = 0.3$ and 0.4) show anomalous temperature dependences due to the development of an energy gap on the FS below $\sim$ 130 and $\sim$ 160 – 190 K. From the X-ray diffraction analysis for $NdO_{1-x}F_xBiS_2$ ($x = 0.25$), the bond angles and lengths of the Bi-S pentahedron change their temperature dependences below $\sim$ 200 K, suggesting the lattice distortion of the Bi-S pentahedron. These results suggest that the lattice instability related to the Bi-S pentahedron below $\sim$ 200 K triggers a CDW transition at lower temperatures. It should be considered that the intrinsic T_c of $NdO_{1-x}F_xBiS_2$ ($x = 0.25$ and 0.4) and $La_{1-y}Sm_yO_{0.5}F_{0.5}BiS_2$ will be much higher than the observed T_c.

Acknowledgments

The authors would like to thank Mr. J. Hayashi of Muroran Institute of Technology for experimental advice and fruitful discussions.

References

1) Y. Mizuguchi, S. Demura, K. Deguchi, Y. Takano, H. Fujihisa, Y. Gotoh, H. Izawa, and O. Miura, J. Phys. Soc. Jpn. **81**, 114725 (2012).

2) J. Xing, S. Li, X. Ding, H. Yang, and H. H. Wen, Phys. Rev. B **86**, 214518 (2012).

3) R. Jha, A. Kumar, S. K. Singh, and V. P. S. Awana, J. Supercond. Novel Magn. **26**, 499 (2013).

4) S. Demura, Y. Mizuguchi, K. Deguchi, H. Okazaki, H. Hara, T. Watanabe, S. J. Denholme, M. Fujioka, T. Ozaki, H. Fujihisa, Y. Gotoh, O. Miura, T. Yamaguchi, H. Takeya, and Y. Takano, J. Phys. Soc. Jpn. **82**, 033708 (2013).

5) G. S. Thakur, G. K. Selvan, Z. Haque, L. C. Gupta, S. L. Samal, S. Arumugam, and A. K. Ganguli, Inorg. Chem. **54**, 1076 (2015).

6) D. Yazici, K. Huang, B. D. White, A. H. Chang, A. J. Friedman, and M. B. Maple, Philos. Mag. **93**, 673 (2012).

7) Y. Mizuguchi, H. Fujihisa, Y. Gotoh, K. Suzuki, H. Usui, K. Kuroki, S. Demura, Y. Takano, H. Izawa, and O. Miura, Phys. Rev. B **86**, 220510(R) (2012).

8) Y. Kamihara, T. Watanabe, M. Hirano, and H. Hosono, J. Am. Chem. Soc. **130**, 3296 (2008).

9) Y. Mizuguchi, J. Phys. Chem. Solids **84**, 34 (2015).

10) M. Nagao, A. Miura, I. Ueta, S. Watauchi, and I. Tanaka, Solid State Commun. **245**, 11 (2016).

11) T. Tomita, M. Ebata, H. Soeda, H. Takahashi, H. Fujihisa, Y. Gotoh, Y. Mizuguchi, H. Izawa, O. Miura, S. Demura, K. Deguchi, and Y. Takano, J. Phys. Soc. Jpn. **83**, 063704 (2014).

12) H. Usui, K. Suzuki, and K. Kuroki, Phys. Rev. B **86**, 220501(R) (2012).

13) X. Wan, H.-C. Ding, S. Y. Savrasov, and C.-G. Duan, Phys. Rev. B **87**, 115124 (2013).

14) A. Miura, M. Nagao, T. Takei, S. Watauchi, I. Tanaka, and N. Kumada, J. Solid State Chem. **212**, 213 (2014).

15) Y. Fang, D. Yazici, B. D. White, and M. B. Maple, Phys. Rev. B **92**, 094507 (2015).

16) M. Nagao, S. Demura, K. Deguchi, A. Miura, S. Watauchi, T. Takei, Y. Takano, N. Kumada, and I. Tanaka, J. Phys. Soc. Jpn. **82**, 113701 (2013).

17) M. Nagao, A. Miura, S. Demura, K. Deguchi, S. Watauchi, T. Takei, Y. Takano, N. Kumada, and I. Tanaka, Solid State Commun. **178**, 33 (2014).

18) L. Jiao, Z. F. Weng, J. Z. Liu, J. L. Zhang, G. M. Pang, C. Y. Guo, F. Gao, X. Y. Zhu, H. H. Wen, and H. Q. Yuan, J. Phys.: Condens. Matter **27**, 225701 (2015).

19) Z. R. Ye, H. F. Yang, D. W. Shen, J. Jiang, X. H. Niu, D. L. Feng, Y. P. Du, X. G. Wan, J. Z. Liu, X. Y. Zhu, H. H. Wen, and M. H. Jiang, Phys. Rev. B **90**, 045116 (2014).

20) T. Yamashita, Y. Tokiwa, D. Terazawa, M. Nagao, S. Watauchi, I. Tanaka, T. Terashima, and Y. Matsuda, J. Phys. Soc. Jpn. **85**, 073707 (2016).

21) Y. Mizuguchi, A. Miura, J. Kajitani, T. Hiroi, O. Miura, K. Tadanaga, N. Kumada, E. Magome, C. Moriyoshi, and Y. Kuroiwa, Sci. Rep. **5**, 14968 (2015).

22) G. Jinno, R. Jha, A. Yamada, R. Higashinaka, T. D. Matsuda, Y. Aoki, M. Nagao, O. Miura, and Y. Mizuguchi, J. Phys. Soc. Jpn. **85**, 124708 (2016).

23) D. Yazici, K. Huang, B. D. White, I. Jeon, V. W. Burnett, A. J. Friedman, I. K. Lum, M. Nallaiyan, S. Spagna, and M. B. Maple, Phys. Rev. B **87**, 174512 (2013).

24) K. Terashima, T. Wakita, M. Sunagawa, H. Fujiwara, T. Nagayama, K. Ono, H. Kumigashira, M. Nagao, S. Watauchi, I. Tanaka, H. Okazaki, Y. Takano, Y. Mizuguchi, H. Usui, K. Kuroki, Y. Muraoka, and T. Yokoya, J. Phys.: Conf. Ser. **683**, 012002 (2016).

25) K. Terashima, J. Sonoyama, M. Sunagawa, H. Fujiwara, T. Nagayama, M. Nagao, S. Watauchi, I. Tanaka, H. Okazaki, Y. Takano, Y. Mizuguchi, H. Usui, K. Suzuki, K. Kuroki, T. Wakita, Y. Muraoka, and T. Yokoya, Phys. Rev. B **90**, 220512(R) (2014).

26) Y. Ota, K. Okazaki, H. Q. Yamamoto, T. Yamamoto, S. Watanabe, C. Chen, M. Nagao, S. Watauchi, I. Tanaka, Y. Takano, and S. Shin, Phys. Rev. Lett. **118**, 167002 (2017).

27) L. K. Zeng, X. B. Wang, J. Ma, P. Richard, S. M. Nie, H. M. Weng, N. L. Wang, Z. Wang, T. Qian, and H. Ding, Phys. Rev. B **90**, 054512 (2014).

28) T. Machida, Y. Fujisawa, M. Nagao, S. Demura, K. Deguchi, Y. Mizuguchi, Y. Takano, and H. Sakata, J. Phys. Soc. Jpn. **83**, 113701 (2014).

29) A. Athauda, Y. Mizuguchi, M. Nagao, J. Neuefeind, and D. Louca, J. Phys. Soc. Jpn. **86**, 124718 (2017).

30) T. Yildirim, Phys. Rev. B **87**, 020506(R) (2013).

31) A. Athauda, J. Yang, S. Lee, Y. Mizuguchi, K. Deguchi, Y. Takano, O. Miura, and D. Louca, Phys. Rev. B **91**, 144112 (2015).

32) J. Kajitani, T. Hiroi, A. Omachi, O. Miura, and Y. Mizuguchi, J. Phys. Soc. Jpn. **84**, 044712 (2015).

33) R. B. Roberts, Philes. Mag. **36**, 91 (1977).

34) H. F. Zhai, Z. T. Tang, H. Jiang, K. Xu, K. Zhang, P. Zhang, J. K. Bao, Y. L. Sun, W. H. Jiao, I. Nowik, I. Felner, Y. K. Li, X. F. Xu, Q. Tao, C. M. Feng, Z. A. Xu, and G. H. Cao, Phys. Rev. B **90**, 064518 (2014).

35) T. Sugimoto, E. Paris, T. Wakita, K. Terashima, T. Yokoya, A. Barinov, J. Kajitani, R. Higashinaka, T. D. Matsuda, Y. Aoki, T. Mizokawa, and N. L. Saini, Sci. Rep. **8**, 2011 (2018).

Table I. Results of EPMA composition analyses and site occupancies normalized by the value at the Nd site in $NdO_{1-x}F_xBiS_2$.

Nominal fluorine concentration x		Nd	Bi	S1 (in-plane)	S2 (out-of-plane)
x = 0.25	Results of EPMA	1.05±0.02	1.01±0.07		
	Normalized site occupancy	1.00	1.00	1.07	1.00
x = 0.4	Results of EPMA	1.04±0.05	0.96±0.05		
	Normalized site occupancy	1.00	0.97	1.06	1.02
x = 0.5	Results of EPMA	1.03±0.06	0.95±0.03		
	Normalized site occupancy	1.00	1.00	1.00	1.13

Table II. Details of structure refinements from ~ 120 to ~ 290 K in $NdO_{0.75}F_{0.25}BiS_2$.

Parameters	Minimum and maximum values
Reflection/Parameter ratio	10.81 ~ 11.44
Residuals : R1(I > 2.00σ(I))	0.0454 ~ 0.0610
Residuals : wR2(All reflections)	0.1304 ~ 0.1728
Goodness-of-fit indicator	1.022 ~ 1.291

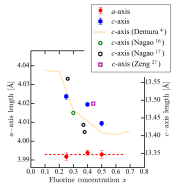

Fig. 1. (Color online) a-axis and c-axis lengths plotted as functions of nominal fluorine concentration x (red solid circles and blue solid hexagons from this work and dotted line from Ref. 4). Also shown are the c-axis length plotted as a function of net x, from Refs. 16 (green open circles), 17 (black open hexagons), and 27 (purple open squares). The red dashed line is a guide to the eyes.

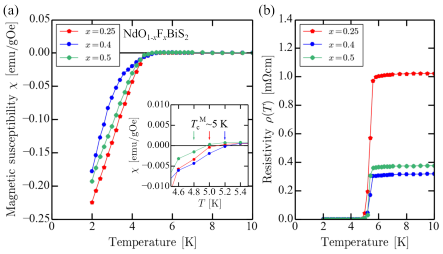

Fig. 2. (Color online) Temperature dependences of (a) magnetic susceptibility and (b) resistivity $\rho(T)$ along the *ab*-plane from 2 to 10 K. The red pentagon, blue hexagon, and green rhombus represent the data for x = 0.25, 0.4, and 0.5, respectively. The arrows in the inset represent T_c^M for x = 0.25 (red pentagon), 0.4 (blue hexagon), and 0.5 (green rhombus).

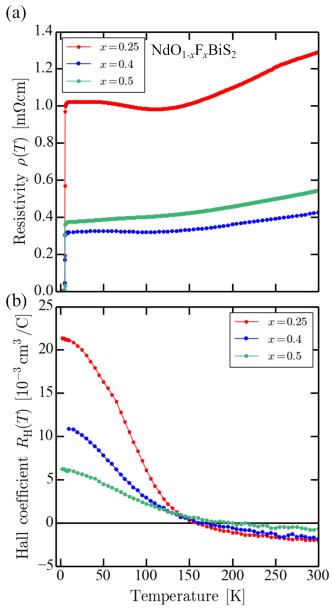

Fig. 3. (Color online) (a) Temperature dependence of resistivity $\rho(T)$ along *ab*-plane from 2 to 300 K. (b) Temperature dependence of Hall coefficient $R_H(T)$ measured under a magnetic field of 5 T applied along the *c*-axis. The red pentagon, blue hexagon, and green rhombus represent the data for x = 0.25, 0.4, and 0.5, respectively.

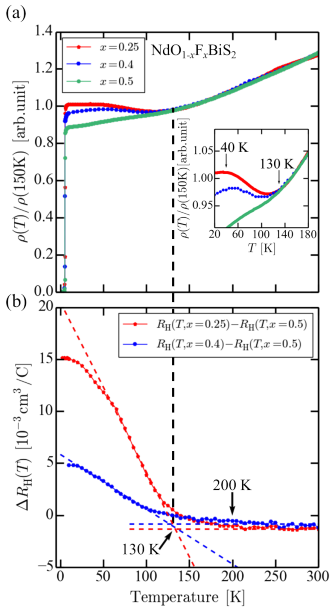

Fig. 4. (Color online) (a) Temperature dependence of resistivity $\rho(T)$ normalized by $\rho(150\ \mathrm{K})$. The inset is an enlargement of the normalized data from 20 to 200 K. (b) Temperature dependence of $\Delta R_\mathrm{H}(T)$. Here, $\Delta R_\mathrm{H}(T)$ is defined by $R_\mathrm{H}(T,x) - R_\mathrm{H}(T,x=0.5)$. The broken lines are fitted to the data below $\sim$ 130 K and above $\sim$ 200 K, respectively. The black broken line is a guide to the eyes.

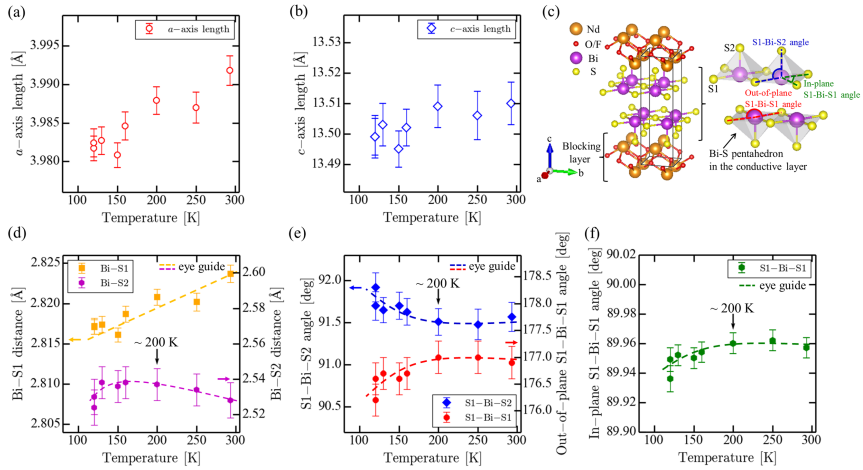

Fig. 5. (Color online) Temperature dependences of (a) *a*-axis length and (b) *c*-axis length for $NdO_{0.75}F_{0.25}BiS_2$. (c) Schematic crystal structures of $NdO_{1-x}F_xBiS_2$ and Bi-S pentahedron. (d) Temperature dependences of the Bi-S1 and Bi-S2 distances, where S1 and S2 represent the in-plane and out-of-plane sulfur, respectively. (e) Temperature dependences of the S1-Bi-S2 bond angle (blue rhombi, left axis) and the out-of-plane S1-Bi-S1 bond angle (red circles, right axis). Here, we define two types of bond angles measured along different directions. One is the in-plane S1-Bi-S1 bond angle and the other is the out-of-plane S1-Bi-S1 bond angle. (f) Temperature dependence of the in-plane S1-Bi-S1 bond angle. The broken lines are the guides to the eyes.

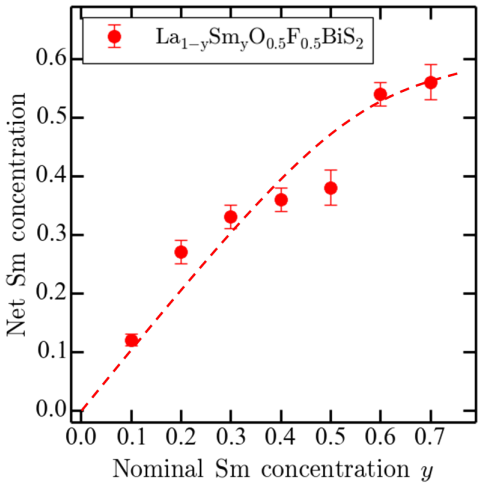

Fig. 6. (Color online) Plot of nominal Sm concentration versus net Sm concentration in $La_{1-y}Sm_yO_{0.5}F_{0.5}BiS_2$. The Sm concentration is estimated using EPMA. The dashed line is a guide to the eyes.

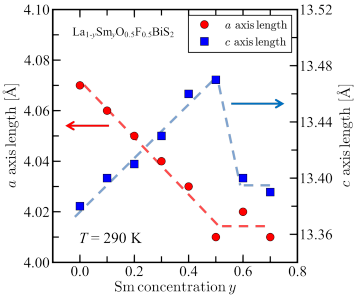

Fig. 7. (Color online) Sm-doping dependence of a-axis and c-axis lengths at ~290 K in $La_{1-y}Sm_yO_{0.5}F_{0.5}BiS_2$. The closed circles and squares are a-axis and c-axis lengths, respectively. The broken lines are guides to the eyes.

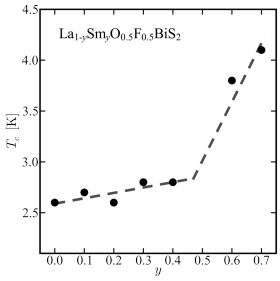

Fig. 8. Sm-doping dependence of T_c in $La_{1-y}Sm_yO_{0.5}F_{0.5}BiS_2$. The broken line is a guide to the eyes.

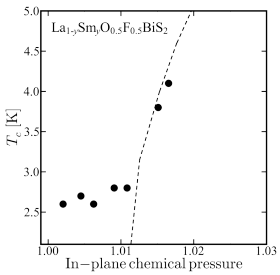

Fig. 9. T_c plotted as a function of in-plane chemical pressure in $La_{1-y}Sm_yO_{0.5}F_{0.5}BiS_2$. The dashed line represents T_c reported by Mizuguchi *et al.*[21)]

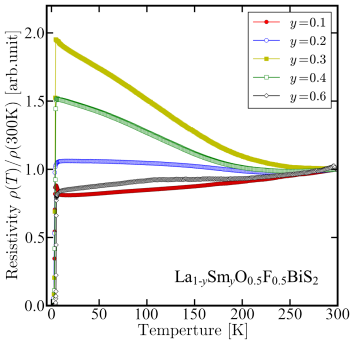

Fig. 10. (Color online) Temperature dependence of resistivity $\rho(T)$ normalized by ρ(300 K) along the ab-plane in $La_{1-y}Sm_yO_{0.5}F_{0.5}BiS_2$ with various Sm concentrations. The data are represented by red solid circles (y = 0.1), blue open circles (0.2), yellow solid squares (0.3), green open squares (0.4), and black open rhombi (0.5).

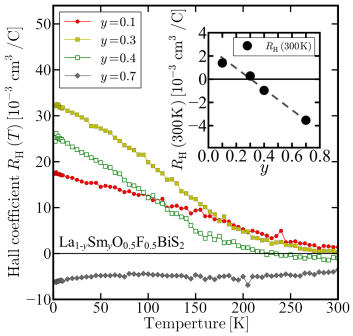

Fig. 11. (Color online) Temperature dependence of Hall coefficient $R_H(T)$ in $La_{1-y}Sm_yO_{0.5}F_{0.5}BiS_2$ with various Sm concentrations, measured under a magnetic field of 5 T applied along the c-axis. The data are represented by red solid circles (y = 0.1), yellow solid squares (0.3), green open squares (0.4), and black solid rhombi (0.7). The inset shows the Sm-doping dependence of R_H(300K).

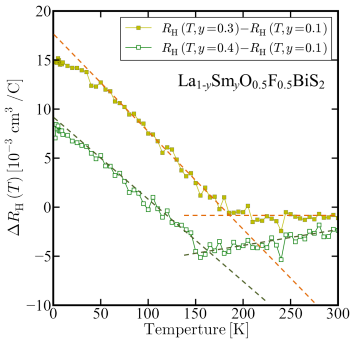

Fig. 12. (Color online) Temperature dependence of $\Delta R_{\rm H}(T)$ in $La_{1-y}Sm_yO_{0.5}F_{0.5}BiS_2$. $\Delta R_{\rm H}(T)$ is defined as $R_{\rm H}(T,y) - R_{\rm H}(T,y=0.1)$. The broken lines are fitted to the linear parts of the data.

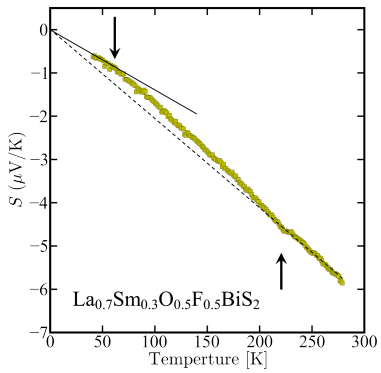

Fig. 13. (Color online) Temperature dependence of Seebeck coefficient $S(T)$ in $La_{1-y}Sm_yO_{0.5}F_{0.5}BiS_2$ with $y = 0.3$. The solid and broken lines, which cross the origin, are fitted to the data at low and high temperature.